J. Phys. D: Appl. Phys. **33** (2000) 2347–2355. Printed in the UK PII: S0022-3727(00)09814-4

Heterodyne force microscopy of PMMA/rubber nanocomposites: nanomapping of viscoelastic response at ultrasonic frequencies

M T Cuberes†‡, H E Assender†, G A D Briggs† and O V Kolosov†

† Department of Materials, University of Oxford, Parks Road, Oxford OX1 3PH, UK
‡ Dpto. Mecánica Aplicada, Universidad de Castilla-La Mancha, Plaza Manuel de Meca 1, 13400 Almadén, Spain

Received 24 November 1999

Abstract. We present measurements of the nanoscale elastic and viscoelastic properties of samples of poly(methylmetacrylate) (PMMA)/rubber nanocomposites. For these studies we have used a new technique based on atomic force microscopy (AFM) with ultrasonic excitation, heterodyne force microscopy (HFM), which provides a means of testing the viscoelastic response of polymeric materials locally (in tip-probed regions) at MHz frequencies. Phase-HFM contrast distinguishes local differences in the dynamic response of PMMA/rubber composites. Comparison of HFM with other AFM-based techniques (ultrasonic force microscopy, friction force microscopy and force modulation microscopy), while imaging the same surface region, emphasizes the unique capabilities of HFM for these kinds of studies, and reveals key nanostructural characteristics of the composites. Some of the toughening particles appear to be broken down, with areas of PMMA detached from the surrounding matrix.

1. Polymer toughened polymers

Polymeric materials are able to show a very wide range of mechanical properties, determined by the orientation and the ease of motion of their component macromolecules. In some instances, the movement of molecular species involves co-operative motion over significant length scales. The viscoelastic nature of polymers means that their response to deformation may be highly dependent upon the time and length scales involved. It is usual for a multiplicity of relaxation processes to be available in response to a change in stress on the material. Where multiple phases and interfaces are present, for example as a result of blending polymers, and in polymer composites and thin film structures, the properties of the interfacial region are often critical to the performance of the material [1]. The mechanical behaviour of polymers at surfaces, interfaces or within nanometre-sized volumes is in general different to that of bulk macroscopic processes. The characterization of the nanoscale morphology and the dynamic mechanical response of interfaces and nanometre-scale volumes provide valuable insight to these issues [2].

The study presented here concerns a nanoscale polymer composite: a rubber toughened polymer acrylic copolymer material. The addition of rubber inclusions into thermoplastics is well-established for improving toughness. In a core-shell PMMA/rubber system, good adhesion between the acrylic matrix—a copolymer based upon poly(methylmethacrylate) (PMMA)—and the rubber is particularly important to achieve high performance. The toughening particles are composed of a core of acrylic enclosed with rubber with a bonded acrylic outer shell. This outer acrylic shell ensures good bonding to the matrix. Study of the nanoscale dynamic behaviour of these materials may help to understand the mechanisms that determine their ultimate impact resistance. The morphology at the surface of the sample is of particular interest as it is in this region where fracture will often initiate. Additionally, because of the rigours of an injection moulding process, the rubber inclusions (especially those close to the surface of the mould) may be distorted, elongated or damaged close to the mould surface where there are high stress and thermal gradients. Such distortions will play an important role in surface-initiated impact resistance.

Scanning force microscopy (SFM) techniques can, to certain extent, address the nanoscale viscoelastic behaviour as well as the nanoscale surface topography and other surface properties, such as adhesion. Such techniques have been applied to the study of polymeric materials. Topographic atomic force microscopy (AFM) images have already shown many morphological details of polymers: chain folding of molecules to form lamellae, spherulitic structures, fibres and different phases in polymer composites and blends, etc [3, 4]. Owing to its capability to probe tip–sample interaction forces, AFM also offers the possibility of investigating

nanoscale material properties [5]. Contrast in friction force microscopy (FFM) of polymer surfaces has been attributed to surface chemistry, molecular orientation, aggregation structure, crystallinity, stiffness and viscoelastic dissipation (molecular relaxation) [6, 7]. Force modulation microscopy (FMM) was specifically introduced for the study of elastic and viscoelastic properties of materials with nanometre-scale resolution [8, 9]. Other AFM-based methods for mapping elasticity and adhesion have also been proposed [10–24], some of them particularly applied to polymer studies [e.g. 15, 21], and developments in scanning probe technology based on thermal analysis techniques have been used to map thermally activated near-surface processes in polymeric materials [25, 26]. The so-called tapping-mode extended the imaging capabilities of the AFM to soft samples, otherwise destroyed by friction and wear in contact-mode scanning [27, 28]. Phase-contrast images in tapping-mode AFM have been related to viscous damping or/and adhesion hysteresis (energy dissipation) [29–31].

To maximize the understanding of polymer nanoscale structure and properties, SFM studies require the application and the careful, self-consistent interpretation of a range of techniques (e.g. AFM, FFM, FMM). New SFM techniques are also needed in order to investigate near surface and subsurface material properties, to extend the range of time constants for mapping viscoelastic response and to avoid damage to the polymer when the tip contacts the sample while probing the mechanical properties. By combining AFM with acoustic characterization, the techniques of ultrasonic force microscopy (UFM) [12, 13] and heterodyne force microscopy (HFM) [22] solve some of the limitations of conventional SFM.

2. Nanomechanical characterization

If you push the tip of a scanning probe microscope into the surface of the sample, and measure how far it moves, then it is possible to characterize the local mechanical properties. What you learn depends on how fast you do this, especially in relation to the resonant frequency of the probe cantilever.

2.1. Force modulation microscopy

The earliest technique applied a frequency well below the tip resonance, and became known as force modulation microscopy [8, 9]). In FMM, the tip is in contact with the sample surface (i.e. the distance between the tip and the sample is such that the force experienced by the tip is in the repulsive regime), and the sample surface is vibrated at a few kHz. The amplitude of tip oscillation at the modulation frequency provides information about the elasticity of the tip-probed sample region. The phase difference between the modulation signal of the sample position and the modulation response of the tip is related to the sample viscoelasticity (loss modulus or energy dissipated during one cycle of excitation).

Using a similar set-up to FMM, it has also been possible to detect surface vibration at higher frequencies (up to several MHz). As in the FMM case, the cantilever-tip experiences an oscillatory force (at the sample modulation frequency) due to the modulation of the tip–sample distance within the repulsive regime of the tip–sample interaction force (which can be considered linear). This procedure for detecting high-frequency surface vibration is designated linear detection, and has been successfully implemented in the so-called acoustic-AFM (A-AFM) [17] and scanning local acceleration microscopy (SLAM) [16] modes for the characterization of nanoscale mechanical properties. Monitoring high-frequency vibration with AFM provides a number of advantages in comparison to working in the FMM mode for the study of material properties. It is possible to obtain information about the contact stiffness (and hence about the local Young modulus) of high modulus materials (like semiconductors, or ceramic materials) using a relatively compliant (highly force sensitive) cantilever; friction is considerably reduced in the presence of high-frequency vibration, and damage is minimized in the imaging of soft delicate samples [12, 13, 16, 32–36].

2.2. Ultrasonic force microscopy

In the limit of very high frequencies of surface vibration, the linear detection mode is not expected to work. Considering the cantilever-tip as a simple point-mass, the amplitude of the sample-induced cantilever-tip vibration vanishes at the ultrasonic regime; the cantilever cannot move fast enough to keep up with surface ultrasonic excitation due to its inertia. Still, it is possible to use a nonlinear detection mode to monitor surface ultrasonic vibration using an AFM tip [12, 13]. If the tip–sample distance is modulated within the nonlinear regime of the tip–sample interaction force, an additional force—the ultrasonic force—-acts upon the cantilever in the presence of ultrasound. This force can be understood as the average force experienced by the tip during an ultrasonic period. Its magnitude depends upon the regime of the tip–sample force that is swept by the tip–sample distance while being modulated at ultrasonic frequencies (i.e. on the initial set-point force, and the amplitude of ultrasound). Owing to the ultrasonic force, the cantilever experiences an additional displacement (ultrasonic response), whose magnitude depends on the details of the tip–sample force, and hence on sample material properties, such as local elasticity and adhesion. If the ultrasonic excitation is modulated at some low kHz frequency, the ultrasonic force varies at the modulation frequency. UFM maps the ultrasonic force at the surface with lateral resolution, providing a means for the nonlinear detection of surface ultrasonic vibration at arbitrarily high frequency. UFM contrast carries information about the sample elastic and adhesive properties, and permits the study of surface and subsurface material properties at the nanometre scale, with the advantages of using high frequency vibration. UFM is implemented on the same apparatus as AFM [33], with appropriate modification. The variation in the measured cantilever deflection as a function of the excitation amplitude is known as the UFM signal.

2.3. Heterodyne force microscopy

HFM also exploits nonlinear detection of ultrasonic vibration. In this case, ultrasound is excited both at the tip (from a transducer at the cantilever base) and at the sample surface (from a transducer at the back of the sample) at adjacent

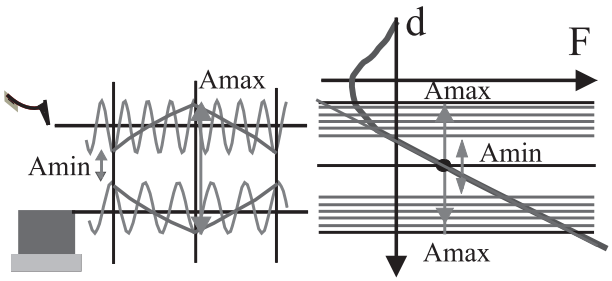

Figure 1. A schematic diagram illustrating HFM. Small phase-delays between tip and sample vibrations (at ω_1 and ω_2 respectively) will cause a phase variation of the cantilever vibration at the difference frequency $\omega_1 - \omega_2$. This is detected as the HFM response.

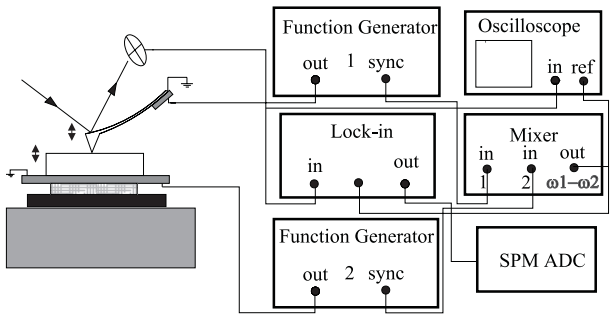

Figure 2. Experimental set-up for HFM. Function generators are used to simultaneously excite ultrasonic vibration at transducers located at the back of the sample and at the cantilever base. Synchronous signals from both generators are electronically mixed, and the output from the mixer is used as a reference signal for the lock-in amplifier.

frequencies, and mixed at the tip–sample gap (see figure 1). As the sample surface vibrates at a frequency ω_1, and the tip at a frequency ω_2, the maximum tip–surface distance is modulated at $\omega_1 - \omega_2$ (beat frequency). Provided that the total amplitude is large enough to cover the nonlinear range of the tip–sample interaction force, an ultrasonic force (stronger for larger amplitudes) acts upon the cantilever, and displaces it from its initial position. Owing to the varying ultrasonic force, the cantilever vibrates at the difference mixed frequency. In HFM, this vibration is monitored in amplitude and phase with a lock-in amplifier, using the (externally) electronically mixed signal as a reference. The information provided by the amplitude-HFM (A-HFM) response is very similar to that obtained by UFM. Nanoscale lateral variations in sample elastic and/or adhesive properties give rise to A-HFM contrast. A unique feature of HFM is its ability to monitor phase shifts between tip and sample ultrasonic vibrations with an extremely high temporal sensitivity (in the ultrasonic time scale). Small differences in the sample dynamic viscoelastic and/or adhesive response to the tip interaction result in a shift in phase of the beat signal that is easily monitored in phase-HFM (ph-HFM). In this way, HFM makes it possible to study dynamic relaxation processes in nanometre volumes with a time-sensitivity of nanoseconds.

The HFM response may be explained in terms of the second-order tip–surface force, F, versus tip–surface distance, z, nonlinearity [22]. In this approximate model the force is given by

$$F(z) = k_s(z_t - z_s) + \chi_s(z_t - z_s)^2 \qquad (1)$$

where z_t and z_s are the instantaneous displacements of the tip and the surface, harmonically vibrating at frequencies ω_t and ω_s respectively, with a phase delay of surface vibration (sample relaxation, resonance or other time dependent phenomena) $\phi = \omega_s^* \tau$ such as $z_t = a_t \cos(\omega_s t)$ and $z_s = a_t \cos(\omega_s t + \omega_s^* \tau)$. Performing straightforward but tedious algebraic manipulations and preserving only the low-frequency terms in the AFM cantilever response, the additional force due to the HF vibrations of the tip and surface is

$$F = \chi_s \left\{ a_t^2/2 - a_s a_t \cos\left[(\omega_t - \omega_s)\, t - \omega_s \tau\right] + a_s^2/2 \right\} \qquad (2)$$

where the first term within the parentheses is responsible for the nonlinear detection of the cantilever vibration (or the waveguide UFM (W-UFM) [23, 36]), the last term describes the nonlinear detection of the sample vibration [12] and the middle term describes the heterodyne mixing of two frequencies [22, 24]. The reason for retaining only the low-frequency terms is that the cantilever and detection system do not respond significantly to the higher frequencies. Since the difference frequency in HFM is set to be below any resonant frequency of the cantilever, and also below any cut-off frequency of the detection system, the deflection of the cantilever is given by this force divided by the cantilever stiffness. As the HF vibration of the sample is detected nonlinearly, with the cantilever HF vibration serving as the local oscillator in the heterodyne analogy, we call this technique the heterodyne UFM, or HFM.

We have implemented HFM on a modified CP-Park AFM. The experimental set-up for HFM is shown in figure 2. PZT ceramic piezos are attached to the sample and the tip holder. Sample and cantilever-tip are bonded to the piezos using a thin layer of crystalline salol (phenyl salicilate). The electrodes of both transducers are connected with soft wires to BNC connectors. Function generators (HP3302) are used to excite their simultaneous sinusoidal vibration at two adjacent (differing in some kHz) frequencies in the MHz range. The function generators provide a synchronous TTL signal with same frequency and phase as that used for excitation. Synchronous signals from both Generators are electronically mixed using a simple electronic mixer, whose output correspond to a triangular wave with the difference frequency. The electronically mixed signal is used as a reference signal for the lock-in amplifier, which monitors vibration of the cantilever at the difference frequency (mixed at the tip–sample gap) in amplitude and phase (HFM response).

3. Results from each technique

Samples of PMMA with core-shell PMMA/rubber inclusions were provided by ICI Acrylics as injected moulded platens. A small piece of the material was cut and bonded to a PZT ceramic piezoelectric transducer using a thin layer of crystalline salol (phenyl salicilate) before mounting on the SFM. The sample thickness was about 3 mm. The smooth (mould face) surface of the sample was uppermost for

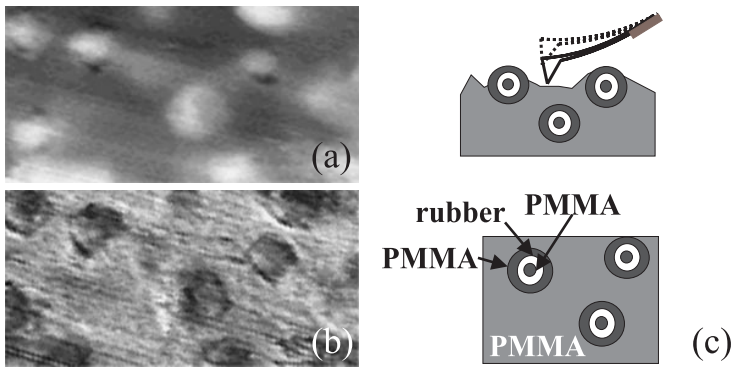

Figure 3. (*a*) Topography in AFM contact mode: 1×0.8 μm; $F_0 = 7$ nN; grey scale range 120 nm. (*b*) Simultaneously recorded W-UFM image: $f = 5.110$ MHz; modulation frequency 2.4 kHz; grey scale range 4 nm. (c) A schematic drawing of the PMMA/rubber sample: upper figure, a representation of a cross-section through the surface; lower figure, a schematic plan view of the surface. The sample surface is not flat. Protrusions in (*a*) reveal the presence of PMMA/rubber/PMMA inclusions in the near-surface region.

imaging. Park Scientific Instruments (Thermal Microscopes) Si ultralevers were used as cantilevers (resonant frequency 25 kHz, spring constant 0.16 N m^{-1}, tip radius 10 nm). The scanning rate was 1 μm s^{-1} unless otherwise indicated. Standard Hertzian analysis can be used to estimate the maximum pressure under a spherical indentor [37]. If the radius of curvature is R, and the reduced elastic modulus is $E^* = E(1-\nu^2)$, and the tip indents the surface by a distance δ, then if surface forces and surface energy are neglected, the maximum pressure under the indentor is

$$p_0 = \frac{2E^*}{\pi}\sqrt{\frac{\delta}{R}}.$$

Putting in illustrative values $E^* = 1$ GPa and $R = 10$ nm (though these values may represent something of a worst case), then if the tip indents the surface by 1 nm the resulting pressure is approximately 200 MPa. Surface adhesion will increase this, and the pressure will also be affected by any non-Hookean behaviour in the polymer. If sliding were to occur with a high coefficient of friction at such a large normal stress then severe damage might be expected. Nevertheless, the experimental observations were that even in the contact mode there was no evidence of cumulative damage following repeated sliding, which mitigates our concern about the magnitude of the contact pressure.

3.1. Atomic force and ultrasonic force microscopy

The PMMA/rubber surface was first examined using conventional contact-mode AFM. Figure 3(*a*) shows a contact-mode AFM image of the surface topography of the PMMA sample with PMMA/rubber/PMMA inclusions. The sample surface is not flat. The protrusions in the image range between 40–120 nm in height. The diameter of the biggest is around 300 nm, which corresponds to the expected diameter of the PMMA/rubber/PMMA inclusions. UFM performed at the same surface region produced the image shown in figure 3(*b*) (recorded simultaneously with figure 3(*a*)). In UFM, the topographic protrusions appear darker, indicative of the presence of a softer material in the near-surface region. UFM contrast depends on sample elasticity and adhesion, and stems from the properties of the nanometre-scale volume probed by the tip when indenting into the sample. Since rubber is much more compliant than PMMA (the moduli of rubber and the PMMA are of the order of 3 MPa and 3 GPa respectively at the working frequencies [1]), we expect a lower UFM signal in regions where some rubber is located at or near to the surface [14].

Changes in the adhesive force related to the tip–surface interaction may also contribute to the image contrast in figure 3(*b*), but considering the strong difference in the stiffness of rubber and PMMA this factor probably dominates. Therefore, we attribute the protrusions in figure 3(*a*) to the presence of PMMA/rubber inclusions at the near-surface region. Figure 3(*c*) shows the elevation and schematic plan of the PMMA/rubber sample, consistent with figures 3(*a*) and 3(*b*). The core-shell rubber inclusions may protrude through the sample surface to different extents. In principle, we do not expect to find rubber directly exposed at the sample surface, since the rubber inclusions in the sample are already covered by a thin PMMA layer when injected in the mould. Close examination of figure 3(*a*) (contact-mode AFM image) reveals some dark spots beside some of the protrusions, which might be cavities, indicative of a lack of adhesion between the PMMA/rubber inclusion and the PMMA matrix, or the absence of a PMMA layer on the toughening particles.

3.2. Friction force microscopy

FFM of the PMMA/rubber sample is presented in figure 4. Figure 4(*a*) is a contact-mode AFM image, simultaneously recorded with FFM images in forward (from left to right) and reversed (from right to left) scans (figures 4(*b*) and (*c*), respectively). Usually, areas where the FFM contrast of forward and backward scans are inverted are attributed to friction variations while areas having same sign of FFM contrast for forward and backward scans are usually attributed to mainly topographical details. The region of the sample, shown in figure 4, appears to contain more defects than the region in figure 3. Small black spots are noticeable both in the AFM and the FFM images. These might arise from cavities on the PMMA matrix surface formed during the sample processing because of defects in the mould. Alternatively, these dark spots may indicate the

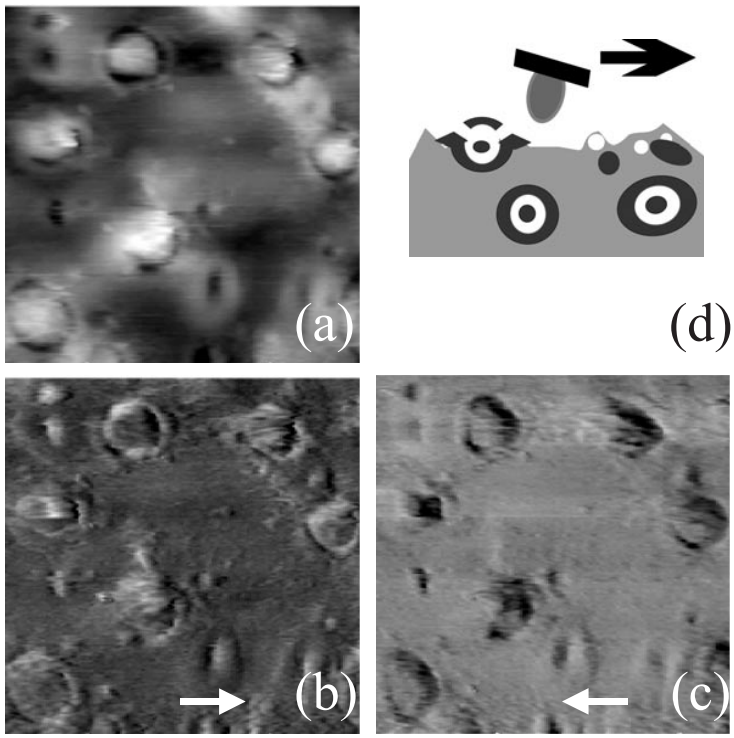

Figure 4. (*a*) Contact-mode AFM image; 2.5 × 2.5 μm; $F_0 = 7$ nN; grey scale range 140 nm. (*b*), (*c*) Simultaneously recorded FFM images scanning (*b*) from left to right, and (*c*) from right to left: sliding velocity 3 μm s^{-1}. (*d*) A schematic drawing of the PMMA/rubber sample consistent with the images (*a*)–(*c*).

presence of rubber at the sample surface, stemming from a broken particle in which rubber has been removed either during moulding or torn off by the tip while scanning. As schematically illustrated in figure 4(*d*) the PMMA/rubber particles may elongate or break during the process of injection of the melt, during which they are subjected to high shear stresses. Dark annular contrast surrounds the large pale protrusions in figure 4(*a*). In principle, this dark annulus might correspond to a cavity surrounding the protrusions, but the high associated friction (figures 4(*b*) and (*c*)) revealing itself as areas with opposite FFM contrast for forward and backward scans suggests rather that it stems from rubber directly exposed at the sample surface. Figure 4(*d*) is a schematic diagram of the PMMA/rubber surface topography that might account for these observations. At some of the PMMA/rubber particles located at the surface, PMMA may be detached from the PMMA matrix, but nevertheless remains attached to the rubber, leaving a halo of rubber exposed at the surface. Alternatively, the whole inclusion may have been sliced in two to expose the central core of PMMA to the surface, surrounded in a shell of rubber. In figures 4(*b*) and (*c*), a halo-shaped frictional contrast is observed at some of the topographic protrusions in both forward (bright halo) and reversed (dark halo) scans, which may be attributed to the presence of rubber directly exposed at the surface. The fact that the contrast on top of the protrusions is very similar to that on the matrix supports the presence of a thin PMMA layer that remains on top of the rubber inclusions. In FFM, a purely topographic protrusion would induce bright (dark) contrast at one side of the protrusion, and dark (bright) contrast at the other side when scanning forwards (backwards). The images in figure 4 were recorded at a scanning velocity of 3 μm s^{-1}, and in the absence of ultrasound. No variations in friction have been observed when increasing/decreasing the scanning velocity between 15 μm s^{-1} and 550 nm s^{-1} [38], however the friction is dramatically reduced when exciting sample and/or tip ultrasonic vibration [32, 33]).

3.3. Force modulation microscopy

The data obtained by FMM on PMMA/rubber are shown in figure 5. Figures 5(*a*) and (*b*) are simultaneously recorded contact-mode AFM and amplitude-FMM (A-FMM) images respectively. Figures 5(*c*) and (*d*) are simultaneously recorded contact-mode AFM and phase-FMM (Ph-FMM) images acquired immediately after figures 5(*a*) and (*b*) in the same region of the surface. In figure 5(*c*) the shape of the bright protrusion has changed with respect to figure 5(*a*) suggesting that the surface is being modified while scanning in the FMM conditions; perhaps the PMMA layer on top of rubber detached from the PMMA matrix is being easily moved and displaced by the tip. In FMM, the tip indents into the surface at kHz frequency while scanning in contact mode, so the surface can be easily damaged by frictional forces. In particular, if the cantilever is slightly tilted with respect to the sample surface, surface vertical vibration results in a horizontal displacement of the tip–sample contact force [39]. Surface modification during scanning makes an unambiguous interpretation of the FMM results difficult. The use of ultrasonic vibration in UFM and/or HFM minimizes frictional effects [32,33]. We did not observe any variation

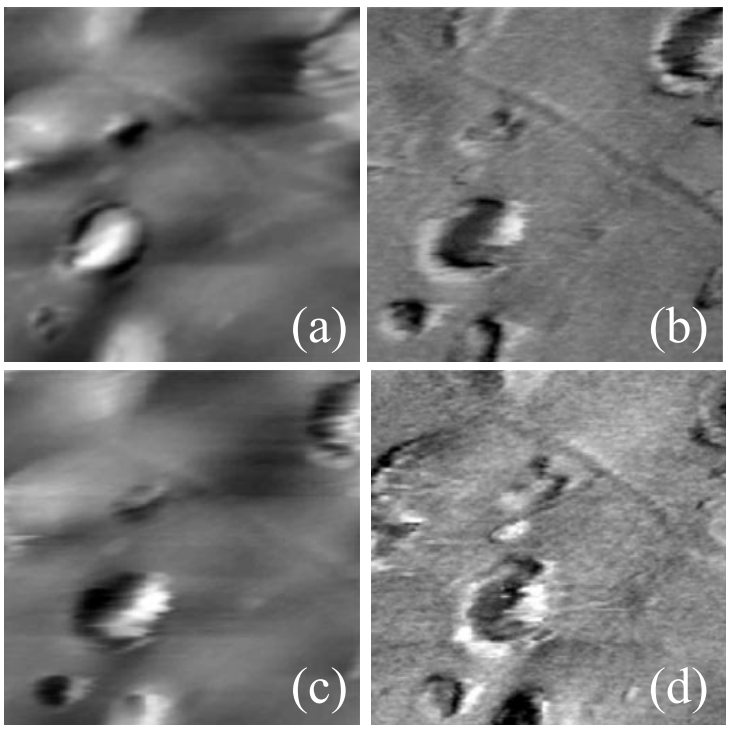

Figure 5. (*a*), (*b*) Simultaneously recorded contact-mode AFM and A-FMM images, and (*c*), (*d*) simultaneously recorded contact-mode AFM and Ph-FMM images: 1.5 × 1.5 μm; grey scale ranges—(*a*), (*c*) 120 nm, (*b*) 3 nm, (*d*) 15°; cantilever stiffness 0.16 N m^{-2}; $F_0 = 7$ nN; sample vibration frequency = 5 kHz.

of the topography when performing UFM and/or HFM in the experimental conditions reported here.

In figure 5(*b*) (A-FMM image), darker contrast is observed over the rubber, consistent with its lower elastic modulus. However, bright areas also appear in the image adjacent to the dark. These may originate because of increases of the tip–sample contact area, perhaps because of tip-induced surface modification. A-FMM is dependent on both the elastic sample properties, and the tip–sample contact area. An increase of the tip–sample contact area leads to an increase of the effective contact stiffness, and hence to a brighter contrast in the image.

In figure 5(*d*) (Ph-FMM image), the contrast in the image is the phase lag of the tip vibration relative to the imposed sample vibration (excitation signal) [3, 9]. Hence, darker contrast generally corresponds to higher energy dissipation. The image shows higher energy dissipation at the protrusions, where there is rubber at the near-surface region. However, as in figure 5(*b*), we also observe areas of brighter contrast next to the dark. Again, variations of the tip–sample contact area, or additional energy due to surface modification may influence the image contrast.

By considering mechanical spectroscopy of the polymers, we can interpret the observed higher energy dissipation of rubber at the tip-probed region compared with PMMA. At 5 kHz, rubber materials of this kind typically have a peak in the loss tangent at around +10°C, with a phase angle of about 60° at its maximum [40]. At this frequency, the glass transition temperature (the α relaxation) of PMMA (associated with a large loss tangent) lies at about 130 °C. PMMA has a secondary loss peak related to a β relaxation (associated to the rotation of the ester $COOCH_3$ side-groups) at around 90 °C at 5 kHz, although this β relaxation has a phase angle of only about 9° at its maximum [1, 41]. Thus at kHz frequencies and ambient temperature, the rubber is expected to have a higher energy dissipation than PMMA. These results correlate with the topography and UFM data1.

3.4. Heterodyne force microscopy

HFM results are presented in figure 6. Figure 6(*a*) is a contact-mode AFM image, figure 6(*b*) is an amplitude-HFM (A-HFM) image, and figure 6(*c*) is a phase-HFM (Ph-HFM) image, recorded immediately afterwards at the same place. Figures 6(*a*) and (*c*) were recorded simultaneously. In figure 6(*b*) (A-HFM), the topographic protrusions appear dark, indicative of the presence of a softer material (rubber) in the near-surface region. The information provided by A-HFM is similar to that obtained from UFM, although the image quality is typically superior in A-HFM. In figure 6(*c*) (Ph-HFM) we find a completely new kind of contrast. The image is recorded with a surprisingly high sensitivity to phase-contrast variations. The grey scale range is of approximately only 5°, (which corresponds to about 2.7 ns time delay, at a vibration frequency of 2 MHz, between brighter and darker areas in the Ph-HFM image). Two different kinds of topographic protrusions may be distinguished in this image: (i) those that give rise to a lower Ph-HFM contrast than the PMMA matrix, and (ii) others that show a Ph-HFM contrast similar to that of the PMMA matrix. These two different protrusions appear similar in figures 6(*a*) and (*b*) (contact-mode AFM and A-HFM images respectively).

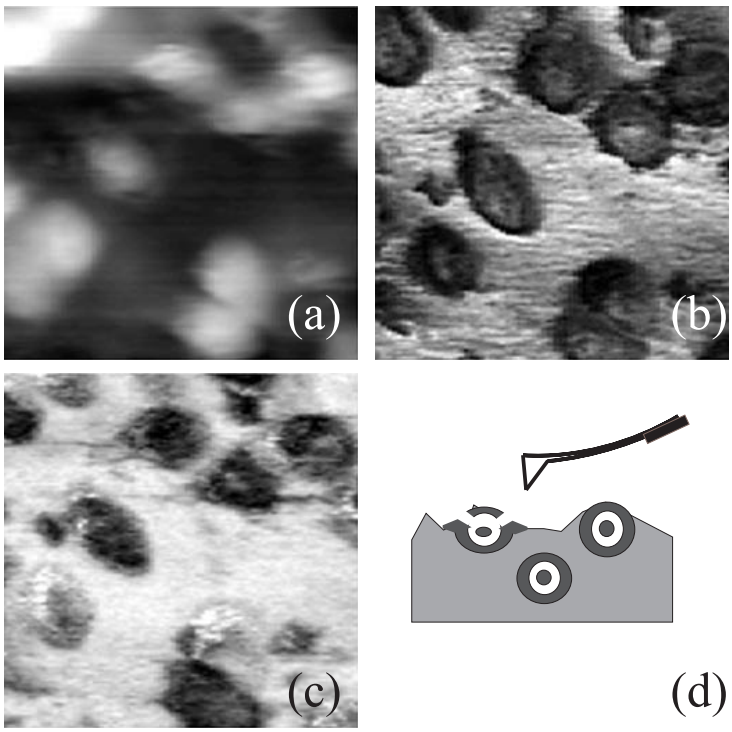

Figure 6. (*a*) Contact-mode AFM, (*b*) A-HFM, and (*c*) Ph-HFM images: 1.5 × 1.5 μm; grey scale ranges—(*a*) 140 nm, (*b*) 2 nm, (*c*) 5° (2.7 ns); $F_0 = 7$ nN; $\omega_1 = 5.110$ MHz; $\omega_2 = 5.120$ MHz. (*d*) A schematic drawing of the topography at the PMMA/rubber sample surface consistent with the results.

The schematic diagram in figure 6(d) illustrates a model for the two different protrusions observed with Ph-HFM. In this illustration, two particles are shown, both of which have a top-most layer of PMMA. The left-hand particle is capped with PMMA that is detached from the matrix materials, but is still attached to the underlying rubber (alternatively, the central PMMA core that is not attached to the matrix PMMA may be exposed). The particle illustrated to the right of the diagram is coated with PMMA that is well adhered to the matrix. It is possible that, on the same surface region, the PMMA on top of rubber is detached from the PMMA matrix at some of the rubber inclusions, whereas at others it remains well adhered to the matrix. The results in figure 6(*c*) may be explained by the existence of these two structures, provided that Ph-HFM contrast is capable of distinguishing between these two situations. As will be shown, a comparative study of Ph-HFM and FFM images on the same surface region demonstrates that there is a correlation of the different structures with the observed differences in HFM. Once this point is demonstrated, the possible mechanisms that may lead to the obtained Ph-HFM contrast will be discussed.

3.5. Using complementary SPM techniques for the interpretation of mechanical nanostructure of PMMA rubber nanocomposites

Figure 7 presents a series of images recorded using different SFM techniques on the same region of a PMMA/rubber sample. Both W-UFM (*b*) and A-HFM (*c*) images reveal a similar contrast, perhaps suggesting the presence of different kinds of islands, even though their topography is qualitatively similar in (*a*). The image quality of (*c*) is arguably better than that of (*b*). As in figure 5, the FMM images (*e*) and (*f*) are not easy to interpret unambiguously, as they are strongly affected by frictional effects, presumably accompanied by variations of the tip–sample contact area (in UFM and HFM friction is strongly reduced by the ultrasound). As in figure 6, the Ph-HFM image (*d*) shows different contrast at protrusions that appear similar in the contact-mode AFM, UFM and A-HFM images. The FMM images (*g*) and (*h*) reveal that those (and only those) protrusions that give rise to a darker contrast in Ph-HFM exhibit the characteristic halo-shaped frictional contrast in forward (bright halo) and reversed (dark halo) FFM scans. This was related to the presence of rubber directly exposed at the sample surface (see figure 4). The other protrusions, however, can be distinguished from the matrix only by FFM, because of features related to their topography that give rise to similar contrast in both forward and reversed scans. All the protrusions appear with the same contrast as the matrix in their central regions when imaged with FFM, indicating that they all have a PMMA surface here. All the protrusions also appear dark by UFM and A-HFM, indicating that they have a layer of rubber at, or just, below, the surface. Therefore, we conclude that the contrast provided by Ph-HFM allows us to distinguish differences in the locally-probed dynamic response of PMMA on top of rubber depending on whether this PMMA is well adhered to the matrix or not.

The mechanisms that lead to phase-contrast involve energy dissipation. Consider again the mechanical spectroscopy arguments such as those discussed for the FMM data in figure 5. With HFM the sample surface is probed at very high frequencies (MHz), therefore, both the loss tangent peak of rubber and the β relaxation peak of PMMA are shifted to higher temperatures, perhaps as high as 30 °C and

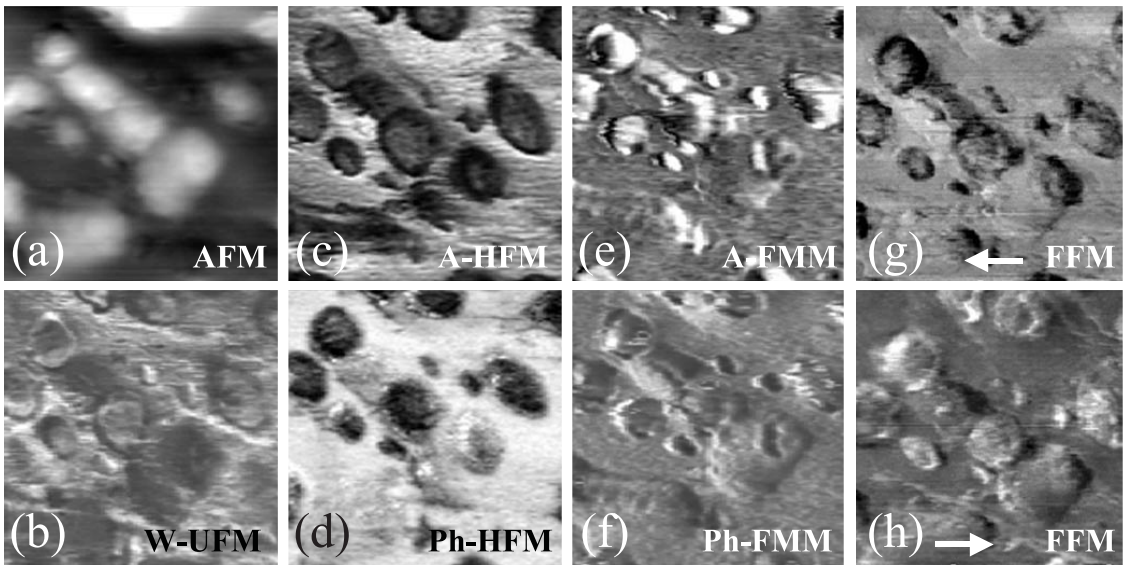

Figure 7. (*a*) Contact-mode AFM (grey scale 140 nm); (*b*) W-UFM ($f = 5.120$ MHz, modulation frequency 2.4 kHz, grey scale 4 nm); (*c*), (*d*) HFM ($\omega_1 = 5.110$ MHz, $\omega_2 = 5.120$ MHz, grey scale—(*c*) 2 nm in A-HFM, (*d*) 5° (2.7 ns) in Ph-HFM); (*e*), (*f*) FMM $f = 10$ kHz (grey scale—(*e*) 3 nm in A-FMM, (*f*) 15° in Ph-FMM); and (*g*) FFM reversed scan; (*h*) FFM forward scan: 1.5×1.5 μm; $F_0 = 7$ nN; scan rate = 1 nm s^{-1} (2 ms/point).

120 °C respectively. It is not apparent, therefore, that such a simple viscoelastic analysis can account for the observed contrast, as one would expect a large difference in phase angle between the rubber and the PMMA matrix regions which is not observed in some of the particles.

A very important difference between FMM and HFM is that in the HFM case, the modulation of the tip–sample distance must necessarily be large enough to cover the nonlinear tip–sample interaction regime. Therefore, when discussing HFM data, it does not seem appropriate to rely only on linear viscoelastic magnitudes such as the storage and loss moduli, and the loss tangent. A dominant contribution to the contrast in Ph-HFM may also stem from nonlinear processes directly related to the mechanical response of the individual molecular chains (intra- or inter-molecular perturbations) upon tip actuation, and/or adhesive dissipative effects of the molecules due to adhesion to the tip, or to other neighbouring molecules.

Dissipative effects that lead to phase-contrast may be related to viscoelastic and/or adhesion hysteresis losses. Such relaxation processes are strongly dependent on the constraints for molecular movement. A different molecular density, entanglement density and/or molecular weight in the PMMA layer on top of rubber that is detached from the PMMA matrix may lead to differences in the PMMA viscoelastic and/or adhesion hysteresis response. In addition, differences in interfacial bonding between the rubber and the PMMA on top, depending on whether the PMMA is well-adhered to the PMMA matrix or not, may also modify the PMMA dynamic behaviour. When probed at very short time scales, the response time measured locally might be strongly affected by small dissipative effects induced by long-range interactions (via molecular entanglements) at molecules outside the immediate contact region. FFM (figures 4(*b*) and 4(*c*) and figures 7(*g*) and 7(*h*)) does not reveal any lateral differences in the viscoelastic and/or adhesion hysteresis behaviour of PMMA. In Ph-HFM we are probing the material with a very high sensitivity, in a very short time scale, and even slight differences in the molecular response time may give rise to noticeable Ph-HFM contrast.

4. Conclusions

The nanoscale elastic properties of rubber toughened PMMA samples can be studied by SFM techniques. The interpretation of the images with respect to the rather complex local structure of the polymer blend is greatly aided by the complementary range of SFM techniques, including UFM and HFM. A-HFM resolves differences in local sample stiffness due to the presence of rubber in the near-surface region. Ph-HFM distinguishes small differences in viscoelastic and/or adhesion hysteresis response time of PMMA on top of rubber. This kind of contrast is unique to Ph-HFM: such differences are not revealed by AFM, UFM, FMM, A-HFM or FFM.

Toughening particles in the polymer penetrate to the surface of an injection moulded component. The internal structure of the core-shell particles is distinguishable by these techniques. In some cases, the toughening particles appear to be broken down, with areas of PMMA detached from the surrounding matrix PMMA, but bonded to the rubber.

Acknowledgments

The authors would like to thank Dr Ian Robinson of ICI Acrylics for the provision of samples and for useful discussions. MTC gratefully acknowledges H M Pollock, F Ouveley, G Gremaud and A J Kulik for useful discussions. This work was supported by EPSRC (GR/L02234).

References

[1] McCrum N G, Buckley C P and Bucknall C B 1988 *Principles of Polymer Engineering* (Oxford: Oxford University Press)
[2] 1996 *MRS Bull.* **21** no 1
[3] Kajiyama T, Tanaka K, Ge S R and Takahara A 1996 *Prog. Surf. Sci.* **52** 1, and references therein
[4] Magonov S N and Reneker D H 1997 *Annu. Rev. Mater. Sci.* **27** 175, and references therein
[5] Burnham N A, Behrend O P, Oulevey F, Gremaud G, Gallo P-J, Gourdon D, Dupas E, Kulik A J, Pollock H M and Briggs G A D 1997 *Nanotechnology* **8** 67
[6] Haugstad G, Gladfelter W L, Weberg E B, Weberg R T and Jones R R 1995 *Langmuir* **11** 3473
[7] Kajiyama T, Tanaka K and Takahara A 1997 *Macromolecules* **30** 280
[8] Maivald P, Butt H J, Gould S A C, Prater C B, Drake B, Gurley J A, Elings V B and Hansma P K 1991 *Nanotechnology* **2** 103
[9] Radmacher M, Tillmann R W and Gaub H E 1993 *Biophys. J.* **64** 735
[10] Cretin B and Sthal F 1993 *Appl. Phys. Lett.* **62** 829
[11] Rohrbeck W and Chilla E 1992 *Phys. Status Solidi* a **131** 69
[12] Kolosov O and Yamanaka K 1993 *Jpn. J. Appl. Phys.* **32** L1095
[13] Yamanaka K, Ogiso H and Kolosov O 1994 *Appl. Phys. Lett.* **64** 178
[14] Dinelli F, Assender H E, Takeda N, Briggs G A D and Kolosov O V 1999 *Surf. Interface Anal.* **27** 562
[15] Dinelli F, Assender H E, Kirov K and Kolosov O V 2000 *Polymer* **41** 4285
[16] Burnham N A, Kulik A J, Gremaud G, Gallo P J and Oulevey F 1996 *J. Vac. Sci. Technol.* B **14** 794
[17] Rabe U and Arnold W 1994 *Appl. Phys. Lett.* **64** 1423
[18] Hirsekorn S, Rabe U and Arnold W 1996 *Europhys. News* **27** 93
[19] Rabe U, Scherer V, Hirsekorn S and Arnold W 1997 *J. Vac. Sci. Technol.* B **15** 1506
[20] von der Werf K O, Putman C A J, Groth B G and Greve J 1994 *Appl. Phys. Lett.* **65** 1195
[21] Rosa A, Hild S and Marti O 1996 *Polym. Preprints* **37** 616
[22] Kolosov O and Briggs G A D 1996 GB Patent Specification 9617380.2
[23] Inagaki K, Kolosov O V, Briggs G A D, Muto S, Horisaki Y and Wright O B 1998 *Proc. IEEE Ultrasonics Symp. (Sendei, Japan, October 1998)* p 1255
[24] Kumano N, Inagaki K, Kolosov O V and Wright O B 1998 *Proc. IEEE Ultrasonics Symp. (Sendei, Japan, October 1998)* p 1269
[25] Hammiche A, Reading M, Pollock H M, Song M and Hourston D J 1996 *Rev. Sci. Instrum.* **67** 4269
[26] Oulevey F, Gremaud G, Sèmoroz A, Kulik A J, Burnham N A, Dupas E and Gourdon D 1998 *Rev. Sci. Instrum.* **69** 2085
[27] Zhong Q, Innis D, Kjoller K and Elings V B 1993 *Surf. Sci. Lett.* **290** L688
[28] Hansma P K *et al* 1993 *Appl. Phys. Lett.* **64** 1738
[29] Tamayo J and Garcia R 1996 *Langmuir* **12** 4430
[30] Tamayo J and Garcia R 1997 *Appl. Phys. Lett.* **71** 2394
[31] Garcia R, Tamayo J, Calleja M and Garcìa F 1998 *Appl. Phys.* A **66** S309
[32] Dinelli F, Biswas S K, Briggs G A D and Kolosov O V 1997 *Appl. Phys. Lett.* **71** 1177
[33] Dinelli F 1998 Ultrasonic force microscopy: surface elastic properties mapping and stiffness evaluation at the nanoscale level *PhD Thesis* University of Oxford
[34] Kolosov O, Briggs G A D, Yamanaka K and Arnold W 1996 *Acoustical Imaging 22* eds P Tortoli and L Masotti (New York: Plenum) p 665
[35] Kolosov O, Ogiso H, Tokumoto H and Yamanaka K 1994 *Nanostructures and Quantum Effects (Springer Series in Materials Science vol 31)* eds H Sakaki and H Noge (Berlin: Springer)
[36] Kolosov O 1998 *Mater. World* (December) 567
[37] Johnson K L 1985 *Contact Mechanics* (Cambridge: Cambridge University Press)
[38] Zwörner O, Hölscher H, Schwarz U D and Wiesendanger R 1988 *Appl. Phys.* A **66** S263
[39] Mazeran P E and Loubet J-L 1997 *Tribol. Lett.* **3** 125
[40] Aklonis J J and McKnight M J 1983 *Introduction to Polymer Viscoelaticity* (New York: Wiley Interscience)
[41] McCrum N G, Read B E and Williams G 1976 *Anelastic and Dielectric Effects in Polymeric Solids* (New York: Wiley)